Available online at www.sciencedirect.com
SCIENCE DIRECT®
Applied Catalysis B: Environmental 59 (2005) 91–98
APPLIED CATALYSIS B: ENVIRONMENTAL
www.elsevier.com/locate/apcatb

Cerium incorporated ordered manganese oxide OMS-2 materials: Improved catalysts for wet oxidation of phenol compounds

M. Abecassis-Wolfovich [a], R. Jothiramalingam [b], M.V. Landau [a], M. Herskowitz [a], B. Viswanathan [b,*], T.K. Varadarajan [b]

[a] *Chemical Engineering Department, The Blechner Center for Industrial Catalysis and Process Development, Ben-Gurion University of the Negev, Beer-Sheva 84105, Israel*
[b] *Department of Chemistry, Indian Institute of Technology, Madras, Chennai 600036, India*

Received 12 October 2004; received in revised form 3 January 2005; accepted 8 January 2005
Available online 5 February 2005

Abstract

Cryptomelane type manganese oxide OMS-2 material was synthesized by redox reaction between potassium permanganate and manganese sulphate in acidic medium under reflux or hydrothermal crystallization conditions. Ce was added by ion-exchange, impregnation or directly at crystallization stage. The chemical composition, structure, texture, morphology and thermal stability of the materials were measured by EDX spectroscopy, XRD, N_2-adsorption, SEM and TGA. Results of the catalytic wet oxidation of phenol at 100 °C indicate best performance of the well-crystallized octahedral molecular sieve with cryptomelane structure where all the accessible potassium ions were exchanged for cerium cations. OMS-2 materials containing pure CeO_2 phase and excess of active oxygen species had lower stability, activity and capacity for oxidative reactive adsorption of phenol. Implementation of Ce-exchanged crystalline OMS-2 catalyst improves the wastewater treatment capacity by a factor of 1.5–2 and 3 compared with co-precipitated Mn–Ce-oxide and activated carbon, respectively.

Keywords: Mn–Ce-oxide catalyst; Cryptomelane; Phenol; Wet oxidation

1. Introduction

Cerium incorporated manganese oxide composite catalyst was widely used in supercritical water oxidation of phenol [1], ammonia [2] and pyridine [3] and in catalytic wet air oxidation of phenol [4,5]. Chen et al. reported a detailed study of composition and activity of manganese cerium mixed oxide composite catalyst by using X-ray diffraction (XRD) and X-ray photoelectron spectroscopy analysis [6]. Microporous manganese oxide octahedral molecular sieve (OMS) material has pore dimensions close to molecular size like zeolites [7,8]. Manganese oxide OMS type materials were widely tested as catalysts in many chemical processes due to their porous structure, mild surface acidity–basicity and ion-exchange ability. Especially, divalent and trivalent transition metal ion incorporated cryptomelane type manganese oxide of OMS-2 type (2×2) matrix (MO-OMS-2) with one dimensional tunnel structure [8] (Fig. 1), has been recently developed as improved oxidation catalyst for alcohols and side chains in organic compounds [9]. Due to its sorption property, MO-OMS-2 is used to remove various radionuclides from nuclear wastes effluents [10]. Hydrophobicity of this type of OMS-2 was successfully exploited for total oxidation of volatile organic compound [11]. Generally, cryptomelane type manganese oxide is produced by reflux method consisting of oxidation of manganese (II) sulphate with potassium permanganate in acidic media. Other methods have also been applied to produce MO-OMS-2 from birnessite type layered material in hydrothermal conditions [12], oxidation of manganese (II) sulphate by potassium persulphate or oxygen [13]. Recently sol–gel route was used by reducing potassium

* Corresponding author. Tel.: +91 44 2578250; fax: +91 44 2578241/8250.
E-mail address: bvnathan@iitm.ac.in (B. Viswanathan).

0926-3373/$ – see front matter © 2005 Elsevier B.V. All rights reserved.
doi:10.1016/j.apcatb.2005.01.001

Nomenclature

C	concentration (g L^{-1} solution)
LHSV	liquid hourly space velocity (h^{-1})
m	mass (g or mg)
P_{O_2}	oxygen pressure (bar)
SRA	selectivity to reactive adsorption of phenol (mg adsorbed phenol/g reacted phenol)
CAC	catalyst capacity to reactive adsorption (mg adsorbed phenol/g cat)
T	reaction temperature (°C)
X	conversion (%)

Sub/superscripts

cat	catalyst
inlet	reactor inlet
outlet	reactor outlet
PhOH	phenol
r	reacted
s	on the surface
TOC	total organic carbon (g of carbon L^{-1})

permanganate with fumaric acid [14]. MO-OMS-2 produced by reflux method has advantages such as higher surface area, smaller particle size and more defects in manganese oxide octahedral lattice that could serve as redox active sites compared to OMS-2 material produced by other synthetic routes. Doping or incorporation of foreign metal particularly divalent or trivalent cations in MO-OMS-2 changes its electronic, catalytic and structural properties [15]. The selection of divalent and trivalent cations was determined by their size, charge and polarizabilities of dopant. MO-OMS-2 with incorporated divalent and trivalent transition metal ions has been proven as a potential catalyst for 2-propanol oxidation and oxidative dehydrogenation of ethanol [15]. Catalytic wet oxidation of phenol using mixed manganese–cerium oxide catalysts was extensively examined both in fixed-bed and batch reactors [4,5], although it was already postulated that this process would be more efficient in a trickle-bed reactor [16–18]. According to [4] the CWO of phenol in a trickle-bed with a bulk mixed oxide Mn–Ce catalyst allows full phenol removal at LHSV $< 10\ h^{-1}$ and 100 °C. Ce incorporated OMS-2 material has never been studied in this process, though its structure and chemical properties discussed above make it a promising catalytic material also for this process. The present study focuses on the effect of synthesis conditions on surface and textural characteristics of cerium incorporated ordered manganese oxide OMS-2 phase and its performance in phenol catalytic wet oxidation reaction compared with a reference co-precipitated (disordered) manganese–cerium oxide catalyst.

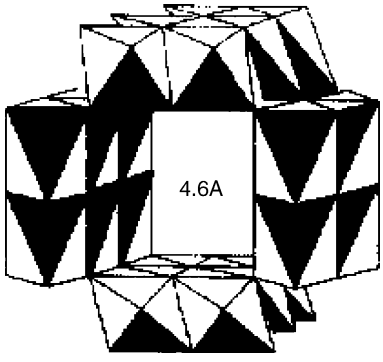

Fig. 1. Structure of potassium incorporated cryptomelane type OMS-2 material [8].

The cerium incorporated porous manganese oxide material was synthesized by ion-exchange process in aqueous medium (reflux and hydrothermal methods) as well as by wet impregnation process. The characterization of cerium incorporated porous manganese oxide OMS-2 materials was done using XRD, TGA, SEM, EDAX and N_2-adsorption methods. The catalysts were tested in catalytic wet oxidation of phenol at moderate reaction conditions in a fixed-bed reactor to examine catalyst oxidation activity, carbon capacity and selectivity towards carbonaceous deposits. The scope of this study was to elucidate the effect of structure of Mn- and Ce-containing phases on the performance of mixed Mn–Ce-oxide catalyst with a given chemical composition.

2. Experimental

2.1. Catalysts preparation

The Ce-dopped ordered Mn-oxide materials with OMS-2 structure were synthesized as follows:

(1) Potassium containing OMS-2 type manganese oxide material was synthesized by oxidation of Mn^{2+} ions in Mn(II)-sulfate solution by permanganate with refluxing in the presence of concentrated nitric acid. The molar ratio between potassium permanganate and manganese sulphate was 0.72 and pH of the reflux solution was maintained at 2–3. Refluxing of the mixed solution was carried out up to 24 h. The product was separated by filtration, washed several times with distilled deionized water and dried at 120 °C overnight [11]. The potassium ions in as-synthesized OMS-2 material were partially exchanged with Ce-ions treating it in 0.25 M aqueous solution of cerium nitrate at room temperature in few cycles (24 h each) with intermediate solid separation and addition of fresh solution of Ce-salt (four cycles to prepare the OMS-2-B catalyst and six cycles for OMS-2-A catalyst). Cerium exchanged OMS-2 material was filtered and washed with distilled water and dried overnight. OMS-2-A sample was then impregnated twice with 0.1 M cerium (III) chloride ($CeCl_3 \cdot 7H_2O$,

Sigma Chemical Co.) aqueous solution by incipient wetness method with intermediate drying at 100 °C to increase Ce in the sample. OMS-2-A-1 material was obtained after the first impregnation and OMS-2-A-2 after the second impregnation. All the samples were calcined at 350 °C in air for 3 h.

(2) Hydrothermal crystallization was employed for direct preparation of cerium incorporated manganese oxide OMS-2 catalyst (OMS-2-C). The cerium incorporated birnessite type manganese oxide layered material was synthesized by alkali route using 5.0 M potassium hydroxide solution as precipitating agent for the formation of $Mn(OH)_2$ suspension where pH of the reaction medium was kept at 12–13. As synthesized $Mn(OH)_2$ suspension was oxidized by dropwise addition of potassium permanganate. The molar ratio of oxidizing agent/Mn(II) was around 0.36 and the mole ratio between Ce(III)/Mn(II) in the reaction mixture was fixed at 0.14 at the initial step by addition of Ce-nitrate salt before oxidizing agent. As synthesized manganese oxide suspension was aged for 4 days at 120 °C. The suspension was washed with distilled water followed by drying at room temperature. The as-synthesized cerium incorporated birnessite with layered structure was ion-exchanged with aqueous solution of 0.25 M Ce(III) ions for few cycles followed by ion exchanged with 0.3 M KCl solution. Finally, potassium and cerium ion-exchanged birnessite material was treated hydrothermally in a teflon coated stainless steel autoclave at 140 °C for 2 days to get Ce-incorporated ordered OMS-2 phase. This sample was calcined at 350 °C in air and denoted as OMS-2-C.

(3) Synthesis of co-precipitated manganese–cerium oxide catalyst (reference catalyst) was conducted by co-precipitation from mixed aqueous solutions of manganese (II) chloride ($MnCl_2{\cdot}4H_2O$, Sigma Chemical Co.) and cerium (III) chloride ($CeCl_3{\cdot}7H_2O$, Sigma Chemical Co.) using NaOH as precipitating agent as described by Imamura et al. [19]. The precipitate with atomic ratio of Mn/Ce = 7/3, close to that in synthesized OMS-2 based materials, was calcined in vacuum at 350 °C as described in [4].

2.2. Catalyst characterization

The chemical composition of the catalysts (average of five data points at different locations of the solid) was measured by energy dispersive X-ray spectroscopy (JEOL JEM 5600 SEM). The SEM micrographs of the materials were obtained with the same instrument.

Surface area and pore volume were derived from N_2-adsorption–desorption isotherms using conventional BET and BJH methods. The calcined samples were outgassed under vacuum at 250 °C. Isotherms were measured at liquid nitrogen temperature with a NOVA-2000 (Quantachrome, version 7.02) instrument.

The phase composition of the catalysts was examined by X-ray diffraction (XRD). The XRD patterns were collected on a Guinier G 670 camera (Cu $K\alpha_1$ radiation) connected with rotating anode X-ray source that was operated at 40 kV and 100 mA. The data were collected in range $2\theta = 3$–70° with step of 0.005°. Exposure time was 30 min. The peak positions and the instrument peak broadening were determined by fitting each diffraction peak by means of APD computer software. The crystal domain size was determined using Scherrer equation $l = K\lambda/[(B^2 - \beta^2)^{0.5}\cos(2\theta/2)]$, were $K = 1.000$, $\beta = 0.1^\circ$, $\lambda = 0.154$ nm and B is the peak broadening at $2\theta = 64.9^\circ$ for cryptomelane phase, $2\theta = 36^\circ$ for Mn_3O_4 oxide and $2\theta = 48^\circ$ for cerium (CeO_2) oxide.

Thermogravimetric analysis (TGA) was carried out on a TA 8200 Mettler Toledo system. The TGA instrument was calibrated with pure iron and nickel. The analyses were performed in Al crucibles (47–52 mg mass) under nitrogen (99.99% purity) with heating rate of 10 °C/min.

2.3. Catalysts performance

The wet oxidation of phenol (Sigma Chemical Co.) was carried out in a trickle-bed reactor as described in [4]. The CWO was performed at 100 °C, 10 bar of oxygen and LHSV = 100 h^{-1}. The testing and analysis procedures were described elsewhere [4]. Tests with glass Raching rings yielded phenol conversion of <1%. Phenol conversion and total organic carbon (TOC) conversion were calculated as: $X_{PhOH}(\%) = (1 - C_{PhOH,outlet}/C_{PhOH,inlet}) \times 100$, $X_{TOC}(\%) = (1 - C_{TOC,outlet}/C_{TOC,inlet}) \times 100$ where C_{PhOH} is phenol concentration and C_{TOC} is TOC concentration.

The total amount of the carbonaceous material adsorbed on the catalyst surface was calculated based on time profile of CO_2 evolution formed during oxidative regenerative treatment after full deactivation as described in [4]. The corresponding mass of phenol deposited at the surface ($m_{PhOH,s}$) was calculated based on this value and compared with the mass of reacted phenol ($m_{PhOH,r}$). The ratio between these two values represents the selectivity towards reactive adsorption (SRA) and was calculated as: SRA = $m_{PhOH,s}/(m_{PhOH,r})$. The catalyst adsorption capacity (CAC) was calculated as: CAC = $m_{PhOH,s}/(m_{cat})$ where m_{cat} is the catalyst mass. Accuracy of SRA and CAC three measurements was 5–10%.

3. Results and discussion

3.1. Chemical, phase composition and textural properties of catalytic materials

XRD patterns of the sample OMS-2-B (Fig. 2a) corresponded to a well-crystallized cryptomelane structure characteristic for the octahedral molecular sieve material OMS-2. The set of (1 0 1), (0 0 2), (3 0 1), (2 1 1), (3 1 0),

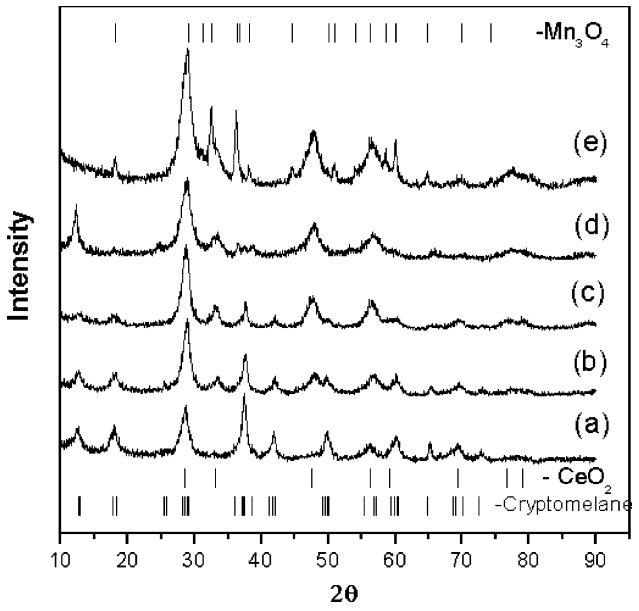

Fig. 2. XRD patterns of synthesized Mn–Ce materials: (a) OMS-2-B, (b) OMS-2-A-1, (c) OMS-2-A-2, (d) OMS-2-C, (e) reference co-precipitated material.

(1 1 4) and (6 0 0) reflections at $2\theta = 12.7$, 18.0, 28.7, 37.4, 41.8, 50.0 and 55.3° and their relative intensities match the patterns of synthetic cryptomelane (KMn_8O_{16}, JCPDS 34-168). The crystal domain size of cryptomelane phase derived from the XRD peaks broadening was 20 nm. No free CeO_2 phase was detected in this sample (absence of reflections at $2\theta = 33.5$ and 48°). The O/Mn ratio of 2.55 (Table 1) in this sample was higher compared with that in pure cryptomelane. This is due to partial exchange of monovalent potassium cations for Ce(III) ions that were hydrolyzed in parent aqueous Ce-nitrate solution forming $Ce(OH)_2^+$ cations and to existence of traces of adsorbed water molecules. Increasing the amount of ion-exchange cycles from four to six only slightly increased the Ce/Mn ratio from 0.034 to 0.037 without significant changes of materials texture parameters (OMS-2-A, Table 1). This could be a result of poor accessibility and/or stronger bonding of remaining potassium ions in cryptomelane framework.

Additional impregnation with Ce-nitrate solution increased the Ce content in OMS-24 and 10 times up to Ce/Mn 0.15 and 0.43 (samples OMS-2-A-1 and OMS-2-A-2, Table 1). Free CeO_2 phase with crystal size of 2–3 nm (Fig. 2b and c) were observed. Increased loading of CeO_2 phase in these samples increased the integral intensity of reflections at $2\theta = 28$, 33.5 and 48° (JSPDS 43-1002) and crystal domain size to 4 nm. No visible degradation of cryptomelane structure was observed. Insertion of additional amount of cerium as CeO_2 nano-particles decreased the surface area from 134 to 103 and then to 94 m^2/g as well as the pore volume (Table 1).

OMS-2-C yielded cryptomelane type structure of lower crystallinity (Fig. 1d) and crystal domain size of 12 nm. The intensities of characteristic reflections in X-ray diffractogram are substantially lower. This sample displayed the highest amount of free CeO_2 oxide phase among all materials with crystal size of 3 nm. Comparison of CeO_2 content derived from XRD data and chemical composition of this sample (OMS-2-C) listed in Table 1 shows that most of ceria is in form of free CeO_2 phase and a small part as exchangeable cations. This correlates with the highest oxygen content in this sample (71.5 at.%, Table 1) that besides extra-oxygen of CeO_2 phase could be a result of higher oxidation state of Mn-ions not included into cryptomelane structure of low crystallinity.

The size and shape of particles forming the texture of synthesized OMS-2 materials strongly depended on the preparation method. The SEM micrographs demonstrated that OMS-2 materials obtained by ‘‘reflux’’ method consisted on relatively large globular particles of 5–25 μm (Fig. 3a) being agglomerates of densely packed small OMS-2 nanocrystals of needle and globular shape clearly visible at higher magnification (Fig. 3b). These particles could be considered as densely packed crystals of octahedral molecular sieve OMS-2 material with domain size 20 nm in agreement with XRD data. This conclusion is consistent with the texture of K-OMS-2 material observed recently with high resolution TEM by Liu et al. [20]. The sample prepared by hydrothermal crystallization represented 0.25–1 μm agglomerates of crystals with globular or needle shape (Fig. 3c and d). This explains the highest surface area (166 m^2/g) and pore volume of OMS-2-C material (Table 1) that could be a result of significant contribution of external surface of small crystals and voids between them, respectively, due to their better accessibility in substantially smaller agglomerates.

Table 1
Chemical, phase composition and textural properties of Mn–Ce catalysts

Catalyst	Surface area ($m^2\ g^{-1}$)	Pore volume ($cm^3\ g^{-1}$)	Phase composition	Elemental composition, EDAX (at.%)				Ce/Mn atomic ratio
				O	K	Ce	Mn	
Reference: co-precipitation [4,16]	96	0.36	Mn_3O_4, CeO_2	62.51	–	11.17	26.31	0.43
OMS-2-B: Ce-ion-exchange, 4 cycles	145	0.41	OMS-2	69.05	2.63	0.95	27.36	0.034
OMS-2-A: Ce-ion-exchange, 6 cycles	134	0.40	OMS-2	67.51	2.60	1.06	28.83	0.037
OMS-2-A-1: Ce-ion-exchange + one Ce-impregnation	103	0.36	OMS-2, CeO_2	64.60	2.56	4.42	28.41	0.15
OMS-2-A-2: Ce-ion-exchange + two Ce-impregnations	94	0.30	OMS-2, CeO_2	62.02	2.42	10.65	24.90	0.43
OMS-2-C: direct hydrothermal synthesis	166	0.51	OMS-2, CeO_2	71.48	0.62	8.60	19.31	0.44

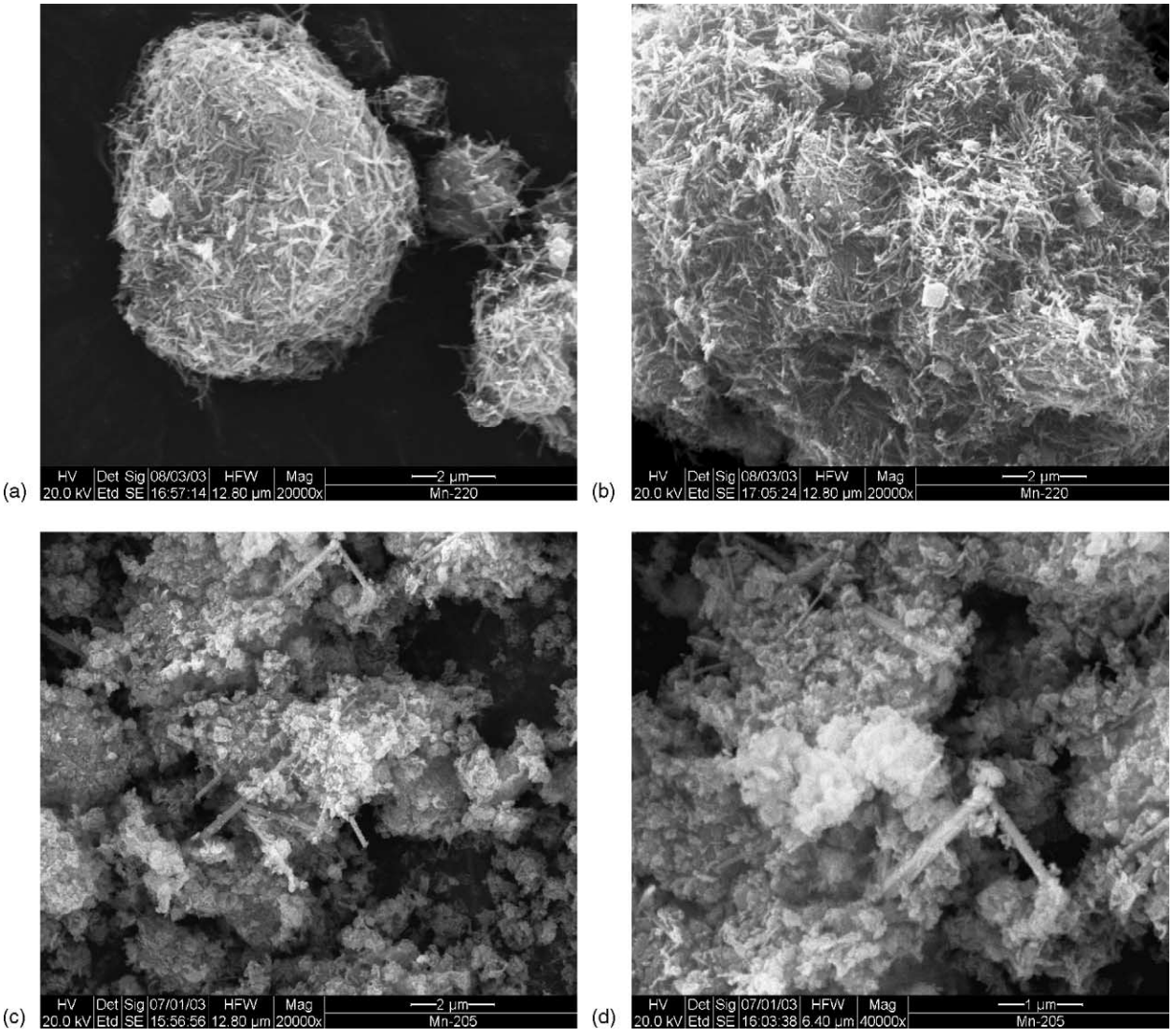

Fig. 3. SEM micrographs of materials OMS-2-A (a and b) and OMS-2-C (c and d).

The reference co-precipitated material with surface area 96 m^2/g, comparable with that measured for Ce-incorporated OMS-2 samples represented a mixture of CeO_2 and Mn_3O_4 nano-particles with crystal size of 7 and 35 nm, respectively, in agreement with the data presented in [4].

3.2. Thermal stability of Ce-incorporated OMS-2 materials

Figs. 4 and 5 represent TGA plots in original and differential forms recorded with ion-exchanged cerium OMS-2-A and OMS-2-C. The thermal stability of the material varied depending on preparation method. For OMS-2-A sample prepared by "reflux" method the first weight loss in range of 30–200 °C was 1.3% and could be attributed to elimination of adsorbed water molecules. The significant weight loss of 7.7% was observed in range 500–800 °C (Fig. 4) and corresponded to the collapse of the tunnel OMS-2 structure confirmed by decreasing of XRD crystallinity in agreement with other data [20].

In Fig. 5 the initial weight loss was observed at 50–100 °C with weight loss of 2.95% due to presence of water molecules present in the porous material. Two more weight losses were observed at the range of 480–750 °C with total weight loss of 7.5%, which is due to decomposition of OMS-2 phase into more stable bixbyite type manganese oxide phase as described at [21].

3.3. Testing of Ce-OMS-2 materials in catalytic wet oxidation (CWO) of phenol

The Ce-incorporated octahedral molecular sieves OMS-2 with different phase composition were tested in phenol CWO and compared with reference co-precipitated Mn–Ce catalyst. The results are presented in Fig. 6 and Table 2. CWO conditions were selected to provide a qualitative

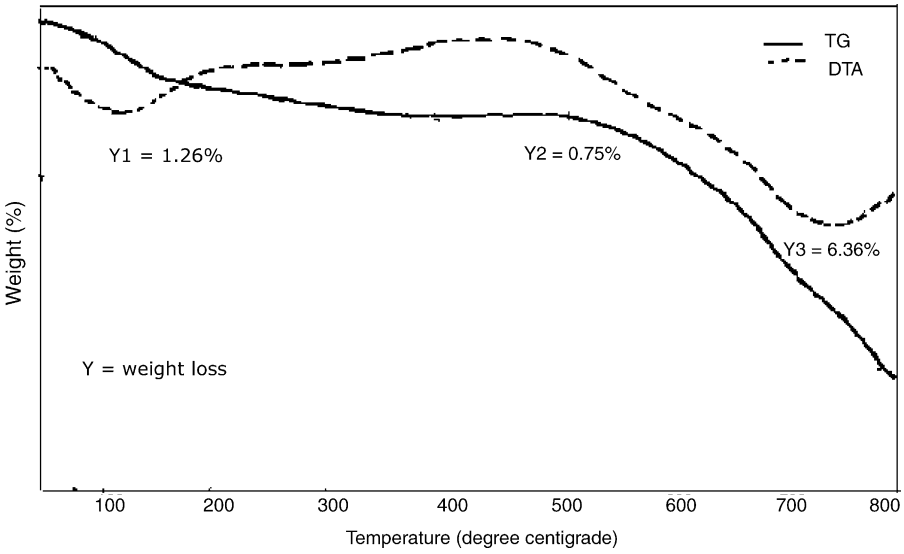

Fig. 4. TGA plots for sample OMS-2-A.

comparison of intrinsic initial activity at 40–60% phenol conversion and deactivation behavior in the range of phenol conversions of 10–60% (Fig. 6). The phenol conversions measured as a function of phenol load at increasing run time at LHSV = 100 h^{-1} showed that Ce-OMS-2 catalysts displayed similar behavior with the reference co-precipitated Mn–Ce-oxide material: after a steady-state period all the catalysts underwent continuous deactivation caused by blocking the catalysts surface with the products of phenol oxidative reactive adsorption [4].

The initial activity of OMS-2-B catalyst being a well-crystallized cryptomelane phase with cerium in form of exchanged cations was comparable with that of reference co-precipitated material. However, its deactivation rate was slower. At the phenol load of 0.6 g/g catalyst the conversion measured with OMS-2-B material was 50% higher than with the reference catalyst (Fig. 6). This yields 70% higher adsorption capacity for reactive phenol adsorption (Table 2). The TOC conversion measured with OMS-2-B catalyst was 1.3 higher than with the reference catalyst reflecting a higher selectivity of oxidative phenol conversion to reactive adsorption route in presence of octahedral molecular sieve catalyst. The slight increase of Ce-content in OMS-2 after additional ion-exchange cycles (sample OMS-2-A) did not affect the performance of the material (not shown). Insertion of additional cerium as free CeO_2 phase by impregnation increased the deactivation rate (Fig. 6) that may be a result of enhancement of the materials basicity [4] and consistent with partial blocking of the OMS-2 pores with occluded CeO_2 phase reflected by decreasing the surface area and pore volume in samples OMS-2-A-1 and -2 (Table 1).

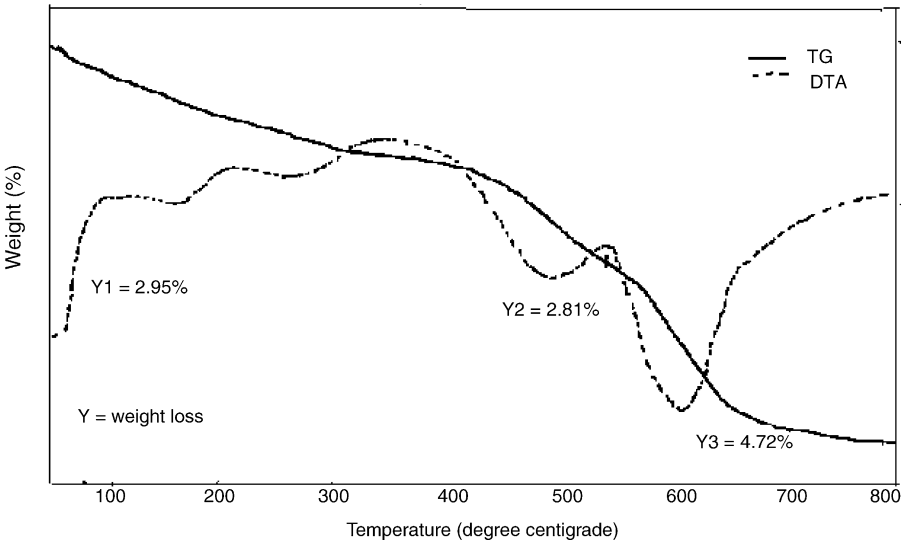

Fig. 5. TGA plots for sample OMS-2-C.

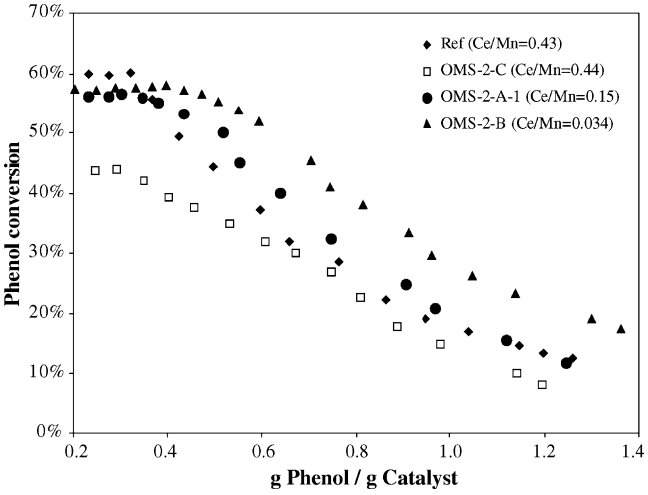

Fig. 6. Performance of Mn–Ce catalysts (LHSV = 100 h^{-1}, T = 100 °C, P_{O_2} = 10 bar).

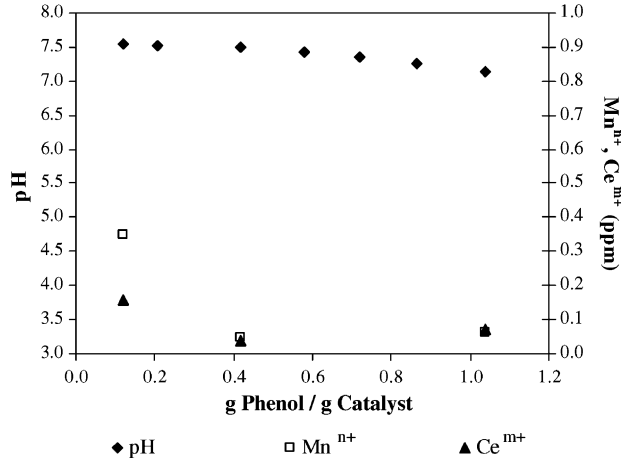

Fig. 7. pH and metal ions concentrations of the effluent during phenol CWO run with OMS-2-B catalyst (LHSV = 100 h^{-1}, T = 100 °C, P_{O_2} = 10 bar).

The OMS-2-C material synthesized by direct hydrothermal crystallization displayed a significantly lower initial activity and completely different CWO selectivity among all the tested samples converting phenol mainly to dissolved oxygenates (10% TOC conversion) in spite of highest surface area (Table 2). This is consistent with high concentration of surface active oxygen species and the lower capacity of this material to reactive phenol adsorption even relative to reference catalyst. The enhanced deactivation reflected by decreasing the steady-state period to 1.1 h may be explained by the fast depletion of surface reactive oxygen that cannot be compensated via reoxidation at low testing temperature of 100 °C, taking into account that this material shows relatively low contribution of reactive adsorption route to phenol conversion.

Testing the OMS-2-B material (that displayed the best performance among the tested catalysts, Fig. 6) after removal of carbonaceous deposits by burning them out, as described in the experimental section, yielded the same performance as demonstrated by the fresh catalyst. The initial phenol conversion was 59%, at TOC conversion of 53%. The regenerated catalyst showed similar values of steady-state period, CAC and SRA as presented in Table 2. This proves a viable opportunity for oxidative-regeneration and recycling of this catalyst. The XRD analysis of the regenerated OMS-2-B material also gave similar patterns as the fresh one evident for thermal stability of its structure. The chemical analysis of the OMS-2-B catalyst after testing and regeneration showed that Ce:Mn:K atomic ratio was 0.035:1:0.1, which is similar to that detected in the fresh catalyst (Table 1). It could be evident for no leaching of metals from the catalysts during the catalyst testing.

This conclusion was confirmed by the analysis of Mn and Ce content and pH in the water effluents taken at different periods of run during OMS-2-B testing, the results of which are shown in Fig. 7. The metal concentration was very low and did not changed between the periods of run corresponding to 0.4 till 1 g phenol/g catalyst in Fig. 6. It means that the gradual reduction of phenol conversion in this period (Fig. 6) is not related to the possible different extent of metal leaching from the catalyst. The pH of initial phenol solution was 6.6. At the beginning of the run the pH of the effluent was 7.5 (close to pure water) due to partial removal of phenol from the solution. The gradual decrease of the pH towards the initial pH value (Fig. 7) correlates with the decreasing of phenol conversion (rising the phenol concentration in the effluent).

All these data show that OMS-2 catalysts are stable at testing conditions from the viewpoints of leaching and structure degradation. It allows attributing all the observed affects to the oxidative conversion of phenol at the solid

Table 2
Performance of Mn–Ce catalysts

Sample number	Initial phenol conversion (%)	TOC conversion (%)	Steady state period (h)	CAC (mg phenol/g cat.)	SRA (mg phenol/g reacted phenol)
Reference	60	43	1.5	300	500
OMS-2-B	58	53	3.2	510	920
OMS-2-A-1	58	52	2.9	485	930
OMS-2-A-2	54	52	2.7	470	940
OMS-2-C	44	10	1.1	220	350

Reaction conditions: LHSV = 100 h^{-1}, $[C_{PhOH}]_0$ = 1 g L^{-1}, T = 100 °C, P_{O_2} = 10 bar.

surface were part of the products remained strongly absorbed by the catalytic material.

The comparison of characterization and phenol CWO testing results of Ce-incorporated OMS-2 materials shows that the well-crystallized OMS-2 material with cryptomelane structure after exchanging of all accessible K-ions for Ce(III) cations displays a combination of high activity, stability patterns and capacity for reactive phenol adsorption. Comparison the performance of this Ce-incorporated octahedral molecular sieve with that of regular co-precipitated Mn–Ce-catalyst [4] and activated carbon materials [22-24] in cleaning of phenol contaminated waste water shows substantial advantage of Ce-OMS-2. At 95–100% of phenol removal that can be achieved with this material at the same conditions by decreasing the LHSV to 1–10 h^{-1} [4] the treatment capacity will be more than 15 L (kg of catalyst)$^{-1}$ h^{-1} versus 7–12 L (kg of catalyst)$^{-1}$ h^{-1} for co-precipitated Mn–Ce-oxide catalysts and 4.6–5.5 L (kg of catalyst)$^{-1}$ h^{-1} for activated carbon [23]. This allows considering the Ce-incorporated OMS-2 type Mn-oxide structures as an improved catalytic material for catalytic wet oxidation of phenol compounds. They have a large potential for further improvements by optimizing the texture parameters and selection of appropriate promoters affecting the efficiency of Mn redox cycle at low temperatures.

4. Conclusions

Cerium incorporated ordered manganese oxide OMS-2 type catalysts containing cerium in the form of exchanged cations and/or pure CeO_2 phase have been synthesized. Best performance in CWO of phenol was observed with well-crystallized octahedral molecular sieve with cryptomelane structure where all the accessible potassium ions were exchanged for cerium cations. OMS-2 materials containing pure CeO_2 phase and excess active oxygen species demonstrated lower performance. Implementation of Ce-exchanged crystalline OMS-2 catalyst increased the water treatment capacity 1.5–2 times compared with co-precipitated Mn–Ce-oxide catalyst and three times relative to activated carbon.

Acknowledgment

The authors would like to thank Professor A. Brenner from the Biotechnology and Environmental Engineering Department, Ben-Gurion University of the Negev for the assistance given in the TOC measurements.

References

[1] Z.Y. Ding, S. Aki, M.A. Abraham, Environ. Sci. Tech. 29 (1995) 2748.
[2] Z.Y. Ding, L. Li, D. Wade, E.F. Gloyna, Ind. Chem. Eng. Res. 37 (1998) 1707.
[3] S. Aki, M.A. Abraham, Ind. Chem. Eng. Res. 38 (1999) 358.
[4] M. Abecassis-Wolfovich, M.V. Landau, A. Brenner, M. Herskowitz, Ind. Chem. Eng. Res. 43 (2004) 5089.
[5] S. Hamoudi, F. Larachi, A. Sayari, J. Catal. 177 (1998) 247.
[6] H. Chen, A. Sayari, A. Adnot, F. Larachi 32 (2001) 195.
[7] Y.F. Shen, R.P. Zerger, R.N. DeGuzman, S.L. Suib, L. McCurdy, D.I. Potter, C.L. O'Young, Science 260 (1993) 511.
[8] C.L. O'Young, R.A. Sawicki, S.L. Suib, Micro. Mater. 11 (1997) 1.
[9] X. Chen, Y.F. Shen, S.L. Suib, C.L. O'Young, J. Cat. 197 (2001) 292.
[10] A. Dyer, M. Pillinger, J. Newton, R. Harjula, T. Moller, S. Amin, Chem. Mater. 12 (2000) 3798.
[11] J. Luo, Q. Zhang, A. Huang, S.L. Suib, Micro. Meso. Mater. 35–36 (2000) 209.
[12] C.C. Chen, D.C. Golden, J.B. Dixon, Clay Clay Mater. 34 (1986) 565.
[13] Q. Feng, H. Kanoh, Y. Miyai, K. Ooi, Chem. Mater. 7 (1995) 148.
[14] N.G. Duan, S.L. Suib, C.L.O. O'Young, J. Chem. Soc. Chem. Comm. 13 (1995) 1367.
[15] X. Chen, Y.F. Shen, S.L. Suib, C.L. O'Young, Chem. Mater. 14 (2002) 940.
[16] A. Pintar, J. Levec, J. Cat. 135 (1992) 345.
[17] A. Pintar, G. Bercic, J. Levec, Chem. Eng. Sci. 52 (1997) 4143.
[18] J. Guo, M. Al-Dahhan, Chem. Eng. Sci. 60 (2005) 735.
[19] S. Imamura, A. Doi, S. Ishida, Ind. Eng. Chem. Prod. Res. Dev. 24 (1985) 75.
[20] J. Liu, Y.-C. Son, J. Cai, X. Shen, S.L. Suib, M. Aindow, Chem. Mater. 16 (2004).
[21] M.I. Zaki, A.K.H. Nohman, G.A.M. Hussein, Y.E. Nashed, Colloid. Surf. A. 99 (1995) 247.
[22] J. Sonyheimer, J.C. Crittenden, R.S. Summers, Activated Carbon for Water Treatment, DVGV-Forschungsstelle, Karlsruhe, Germany, 1988.
[23] U.S. EPA, Wastewater Technology Fact Sheet, Granular Activated Carbon Adsorption and Regeneration, U.S. EPA 832-F-00-017, Washington, DC, 2000.
[24] Y.I. Matatov-Meytal, M. Sheintuch, Ind. Eng. Chem. Res. 36 (1997) 4374.